

Multiparameter MRI assessment of normal-appearing and diseased vertebral bone marrow

Andreas Biffar¹, Andrea Baur-Melnyk², Gerwin P. Schmidt², Maximilian F. Reiser^{1,2}, Olaf Dietrich¹

¹ Josef Lissner Laboratory for Biomedical Imaging, Institute of Clinical Radiology, LMU University Hospitals Munich-Grosshadern, Germany

² Institute of Clinical Radiology, LMU University Hospitals Munich-Grosshadern, Germany

ELECTRONIC PREPRINT VERSION:

Not for commercial sale or for any systematic external distribution by a third party

The original publication is available at <<http://www.springerlink.com>>.

Final version: European Radiology 2010; 20: 2679–2689. <URL:<http://dx.doi.org/10.1007/s00330-010-1833-4>>

Abstract

Objective: To evaluate spin-lattice (T1) and spin-spin (T2) relaxation times as well as apparent diffusion coefficients (ADCs) of the fat and water components in the vertebral bone marrow (vBM) of patients with benign and malignant lesions.

Methods: 44 patients were examined at 1.5 T: (1) 24 osteoporotic vertebral fractures (15 women, 9 men, median age: 73, range: 48–86 years) and (2) 20 malignant vertebral infiltrations (9 women, 11 men, median age: 60, range: 25–87). Relaxation times were determined separately for the water and the fat component using a saturation-recovery technique for T1 and measurements with variable echo time for T2. ADCs were determined with a diffusion-weighted (DW) echo-planar imaging (EPI) and a single-shot turbo-spin-echo (ssTSE) sequence.

Results: T1 of the water component and ADCs were significantly increased in the lesions compared with normal-appearing vBM (malignant: 1252 vs. 828 ms, osteoporotic: 1315 vs. 872 ms). ADCs determined with the DW-ssTSE were significantly increased compared with the DW-EPI. ADCs determined with the DW-ssTSE differed significantly between osteoporotic and malignant lesions (1.74 vs. 1.35×10^{-3} mm²/s).

Conclusions: All parameters exhibit significant differences between normal-appearing vBM and the lesions. However, only the ADCs determined with the DW-ssTSE differed significantly between osteoporotic fractures and malignant lesions potentially allowing for a differential diagnosis of these two entities.

Keywords: magnetic resonance imaging; relaxation times; diffusion; vertebral bone marrow; vertebral fractures

Corresponding author:

Olaf Dietrich, PhD
Josef Lissner Laboratory for Biomedical Imaging,
Department of Clinical Radiology
LMU University Hospitals Munich-Grosshadern
Marchioninstr. 15, 81377 Munich
Tel.: +49 89 7095-4622, Fax: +49 89 7095-4627,
e-mail: od@dtrx.net

Introduction

Magnetic resonance imaging (MRI) plays an integral role in the detection and characterisation of bone marrow lesions. The evaluation of pathological features of vertebral bone marrow (vBM) with MRI is performed using standard T1- or T2-weighted and short-tau inversion-recovery (STIR) sequences.

The signal characteristics of vBM are mainly dominated by the distribution pattern of its constituents, namely yellow and red marrow [1]. Yellow marrow mainly consists of fat, while red marrow consists of comparable amounts of fat and water. Image contrast in MRI depends on the relaxation characteristics and in diffusion-weighted (DW) sequences also on the diffusion coefficients of the underlying tissue. These characteristics are known to be different for protons in water and fat. Fat exhibits a very efficient spin-lattice relaxation resulting in a short T1 relaxation time [2] and a relatively long T2 relaxation time [3]. T1 of the water component is relatively long compared to the fat component, while T2 is shorter [4]. The diffusivity, measured in terms of the apparent diffusion coefficient (ADC), of fat protons is almost negligible while it is very high in water. Bulk T1 and T2 relaxation times [5-7] and ADCs [8-12] of vBM were determined in various studies, reflecting average parameters of both components without permitting them to be separated. Only few studies separately determined the parameters for the fat and water components in normal vBM as well as in pathological conditions [13-15].

Benign (osteoporosis) or malignant (tumor or metastasis) causes of acute vertebral collapse are often difficult to differentiate. An accurate diagnosis is important for appropriate treatment and prognosis. Studies based on signal intensities in STIR or non-contrast-enhanced and contrast-enhanced T1-weighted images as well as on morphological characteristics of the lesions [16-22] have been performed, yielding promising results with accuracies up to 95%. However, these results are based on qualitative criteria, depending on the sequence setup and the experience of the reader. Since both pathologies are expected to change the tissue physiology differently, quantitative imaging might therefore be able to differentiate between benign and malignant lesions and overcome the limitations of qualitative criteria. T2 [14, 23, 24], T1 [14, 23], and especially the ADC [25-31] were evaluated in this context.

The purpose of the present study was the separate measurement of ADC, T1, and T2 of the fat and water components. Measurements were performed in patients with normal-appearing vBM as well as with benign and malignant vertebral lesions in order to analyse the effects of various pathological processes on the physical properties of the bone-marrow components.

Materials and Methods

Patients

After internal review-board approval and informed consent had been received 44 patients were examined. Patients were divided into groups according to the cause of the acute vertebral fracture. Group 1 consisted of 24 benign fractures in 24 patients with osteoporosis (15 women and 9 men, median age: 73 years, range: 48–86 years). The presence of a tumour in these patients was ruled out by follow-up MR examinations or multidetector computed-tomography (CT) examinations. Group 2 consisted of 20 malignant infiltrations in 20 patients (9 women and 11 men, median age: 60 years, range: 25–87 years) accompanied by pathological fractures in 12 of these 20 cases. Primary neoplasms included multiple myeloma (n=7), breast cancer (n=5), adenocarcinoma (n=3), ovarian cancer (n=1), hypopharyngeal cancer (n=1), thyroid carcinoma (n=1), bladder cancer (n=1) and non-seminoma (n=1). The diagnoses were confirmed with histopathological examination of specimens obtained during surgery, CT-guided biopsy, or follow-up MR examinations. Patients without an acute bone-marrow oedema in fracture sites were excluded.

Magnetic Resonance Imaging

Measurements were performed on a 1.5-Tesla whole-body system (MAGNETOM Avanto, Siemens Healthcare, Erlangen, Germany) using a quadrature spine surface coil. T1-weighted (TR/TE, 531/12 ms), STIR (TR/TE/TI, 3790/61/180 ms) and T2-weighted (TR/TE, 4420/118 ms) turbo-spin-echo images of 21 sagittal slices with a slice thickness of 3.0 mm were acquired using a 44×44 cm² field of view (FOV) and a matrix size of 384×384 and used for lesion localisation and proper slice positioning in the following measurements.

A sagittal slice centred on the lesion with a slice thickness of 5.0 mm and a FOV of 30×22 cm² was selected. First, ADCs were determined with a fat-saturated diffusion-weighting single-shot turbo-spin-

echo (DW-ssTSE) sequence (TR/TE, 3000/72 ms) with 4 different b-values ($b=100, 250, 400, 600 \text{ s/mm}^2$) and matrix size: 128×92, flip angle: 180° for the refocusing pulses, and a bandwidth of 735 Hz/pixel. Diffusion gradients were applied in all three physical gradient directions simultaneously to achieve a maximum gradient amplitude and diffusion weighting. Because of the low signal of the bone marrow in DWI, ten averages were taken in order to improve the signal-to-noise ratio (SNR). Second, a fat-saturated diffusion-weighted echo-planar imaging (DW-EPI) sequence (TR/TE, 3000/87 ms, $b=50, 300, 600 \text{ s/mm}^2$) was performed with a matrix size of 192×144 and a bandwidth of 965 Hz/pixel. The diffusion signals were averaged over 5 repeated acquisitions and 3 orthogonal gradient directions. In both measurements, the b-value was varied by a change of the diffusion-gradient amplitude keeping the gradient duration constant.

T1 of the water and fat component were determined with a saturation-recovery (SR) half-Fourier-acquisition single-shot turbo-spin-echo (HASTE) sequence (saturation times TI=5, 50, 100, 200, 400, 800, 1600, 3200 ms) preceded by either a fat- or water-saturation pulse, respectively. T2 was measured using a HASTE sequence with varying echo times (TE=14, 28, 69, 99, 130, 170 ms) preceded by either a fat- or water-saturation pulse, respectively. The matrix size was 128×92 pixels and the bandwidth 735 Hz/pixel. TE was fixed to 14 ms for the T1 measurements and TR was fixed to 2500 ms for the T2 measurements with variable TE. In both cases, 2 averages were acquired for each TI or TE.

Post-processing

The data was post-processed offline on a personal computer using in-house-built software PMI 0.4 [32].

Parameters were determined in patients with benign and malignant lesions. In the case of T1 and T2, values of water and fat were measured separately. The diffusivity of the fat component is negligible ($\text{ADC}_{\text{fat}} < 0.1 \times 10^{-3} \text{ mm}^2/\text{s}$) [13] and was not measured.

Vertebrae were classified as normal or abnormal-appearing according to their appearance on T1-weighted and STIR images by the consensus decision of two experienced radiologists (A.B., G.S.). An acute fracture was defined as a hyperintense region on the STIR images. Old fractures (without any signs of vBM oedema, i.e. hyperintensity on the STIR image) or diffusely infiltrated vertebrae (manifested as

a homogeneous signal reduction on unenhanced T1-weighted images) were excluded.

ROIs for T1 quantification were selected manually in the lesions on the fat-saturated image with the longest saturation time and in the normal-appearing vertebrae on the water-saturated image with the longest saturation time, providing the best contrast between vertebral bodies and intervertebral discs. T1 was calculated fitting signal intensities of the ROIs for varying TI to a monoexponential saturation-recovery model [33]. The ROIs from the T1 quantification were used for T2 quantification and corrected manually if necessary. T2 was quantified, fitting signal intensities for varying TE to a monoexponential decay model [34].

For ADC quantification, the same ROIs were used and corrected manually according to their appearance on the image with the lowest diffusion weighting. Signal intensities for varying b-values were fitted to a monoexponential decay model using a least-squares algorithm to determine ADCs [35].

In addition, parameter maps were calculated by determining the value of each parameter on a voxel basis.

Statistical Evaluation

Mean values and standard deviations of the parameters for both types of lesions and for normal-appearing vBM were determined. To compare normal-appearing vBM and lesions within one patient group, a paired two-tailed t-test was performed. To compare parameters in normal-appearing vBM and lesions between both patient groups, an unpaired two-tailed t-test was performed.

In each patient, the intrapatient variability (IPV) of each parameter was calculated. It was defined as the standard deviation of a parameter over all normal-appearing vertebrae per patient (evaluating one ROI for each vertebra). The values were normalised to the mean value in normal-appearing vBM of the corresponding patient. The ratio between the mean value in normal-appearing vBM and the lesion was calculated.

Correlations between T1, T2, and ADC measurements were assessed using Pearson's product-moment correlation coefficient and its significance was determined using a one-tailed paired t-test.

Accuracies, specificities, and sensitivities of the parameters for the detection of malignant lesions (to be differentiated from osteoporotic (benign) lesions)

were calculated. As a cut-off value, the parameter yielding the highest accuracy was chosen. To analyse whether a combined classification based on two parameters increases the accuracy, Fisher's linear discriminant analysis was performed.

Results

Parameter maps for each parameter were calculated and exemplary images are shown in Figs. 1 and 2. For the subsequent statistical analysis, the parameters were determined on a ROI basis. In total, 12 pathological fractures, 8 malignant infiltrations (tumour or metastasis), and 24 osteoporotic fractures were evaluated. Additionally, 68 ROIs in normal-appearing vBM in patients with malignant lesions

and 147 ROIs in patients with benign lesions were evaluated. In 6 patients with a malignant lesion, all vertebrae showed signs of diffuse infiltration and hence a determination of values in normal-appearing vBM was not possible. T1 and T2 relaxation times of the fat component could not be determined in the lesions, as the water-saturated signal was too low because of a negligible fat fraction. In two patients with malignant lesions, the T2-values of water could not be evaluated because of poor image quality. In one patient with a malignant lesion, the DW-EPI sequence could not be evaluated because of poor image quality. Exemplary fits of the ROI data to the different models for ADC, T1, and T2 quantification are shown in Figs. 3 and 4.

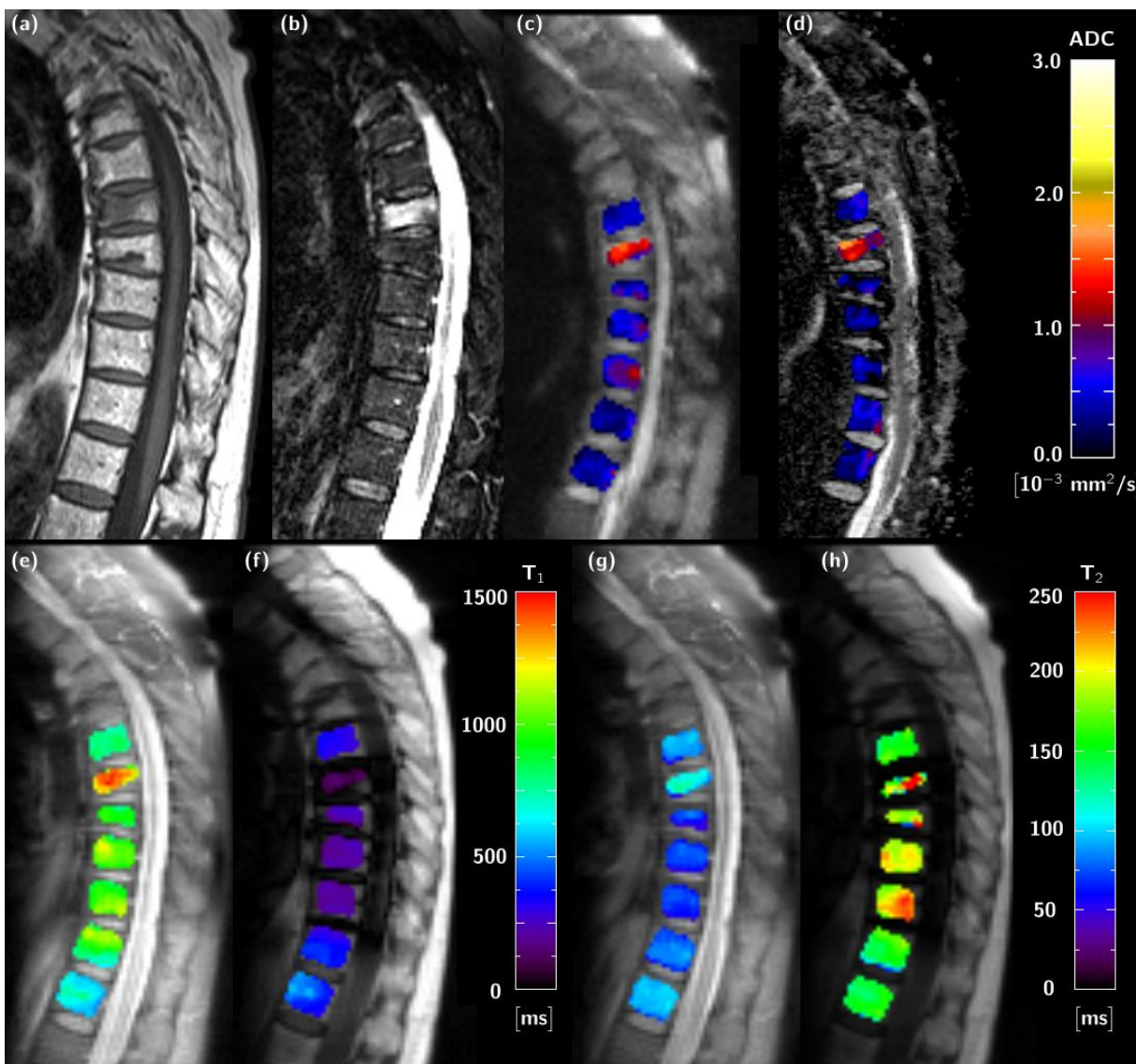


Figure 1: (a) T1-weighted TSE and (b) STIR images of a patient with an osteoporotic fracture in T7 and the corresponding parameter maps of the ADC determined with (c) the DW-ssTSE and (d) the DW-EPI sequence as well as the (e) T1 water, (f) T1 fat, (g) T2 water and (h) T2 fat are shown.

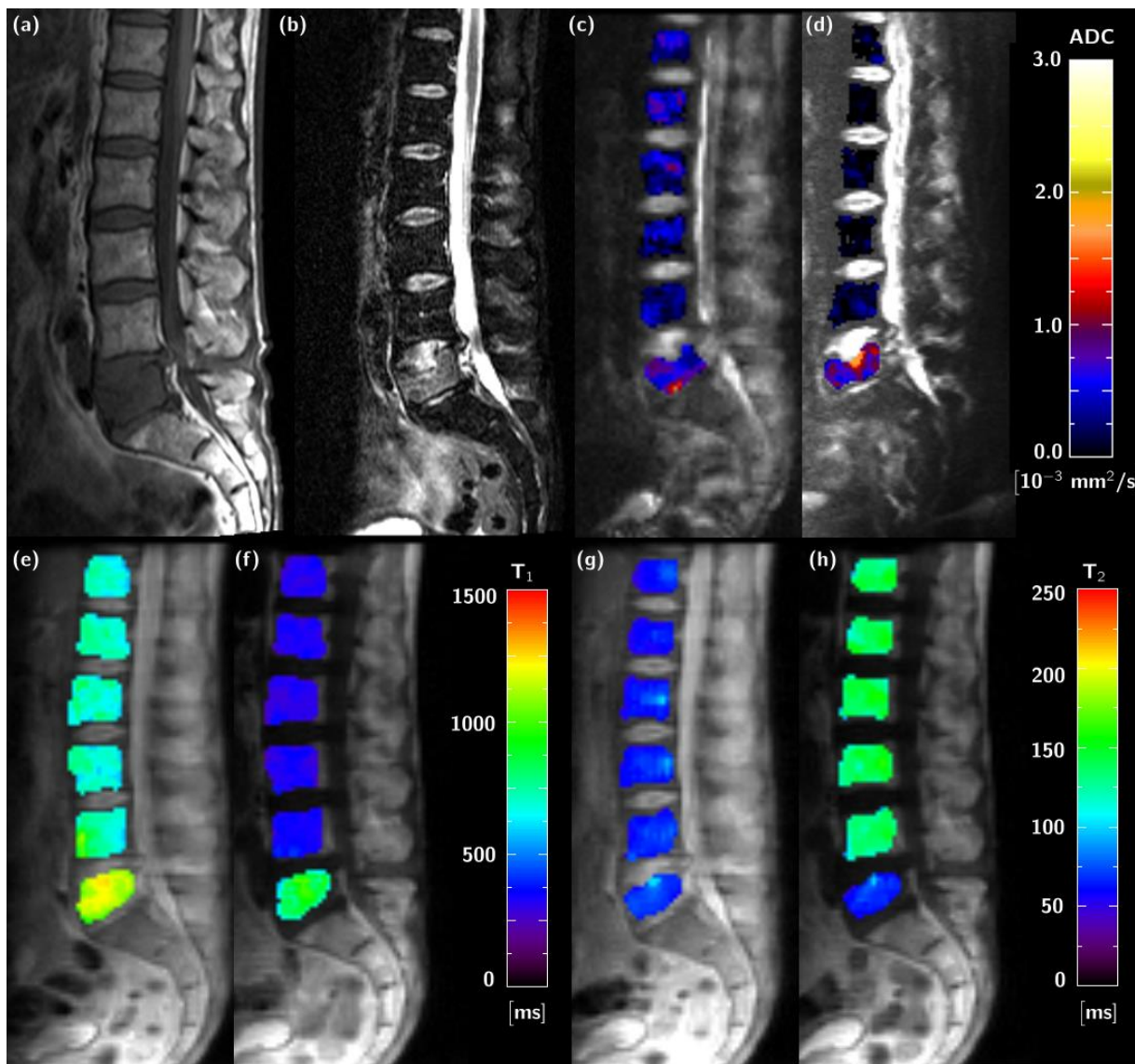


Figure 2: The same images as in Fig. 1, but for a patient with a malignant lesion in L5.

Table 1: Summary of T1, T2, and ADC values in normal-appearing vBM and in lesions of patients with malignant infiltrations or benign osteoporotic fractures. The mean values are shown together with the standard deviations in parentheses

Tissue	Parameter	T1 [ms]		T2 [ms]		ADC [10^{-3} mm ² /s]	
		Water	fat	water	fat	DW-ssTSE	DW-EPI
Normal-appearing vBM							
	Malignant (n=147)	878 (177)	386 (144)	99 (26)	146 (30)	0.62 (0.22)	0.35 (0.17)
	Osteoporotic (n=68)	872 (129)	324 (81)	88 (16)	163 (32)	0.58 (0.17)	0.31 (0.15)
Pathological condition							
	Malignant (n=24)	1252 (157)	--	107 (26)	--	1.35 (0.41)	1.06 (0.19)
	Osteoporotic (n=20)	1315 (163)	--	122 (25)	--	1.74 (0.25)	1.17 (0.37)

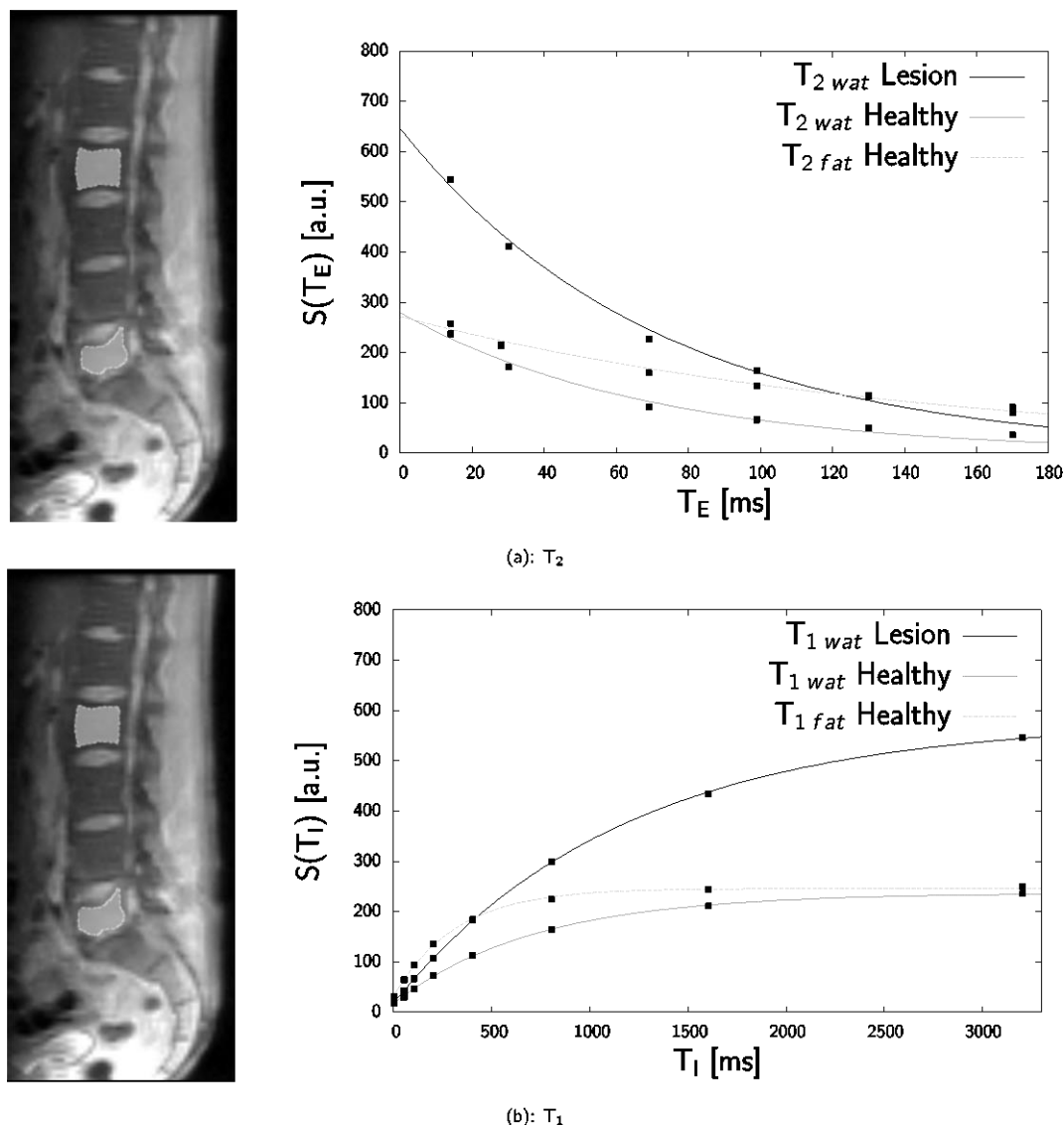
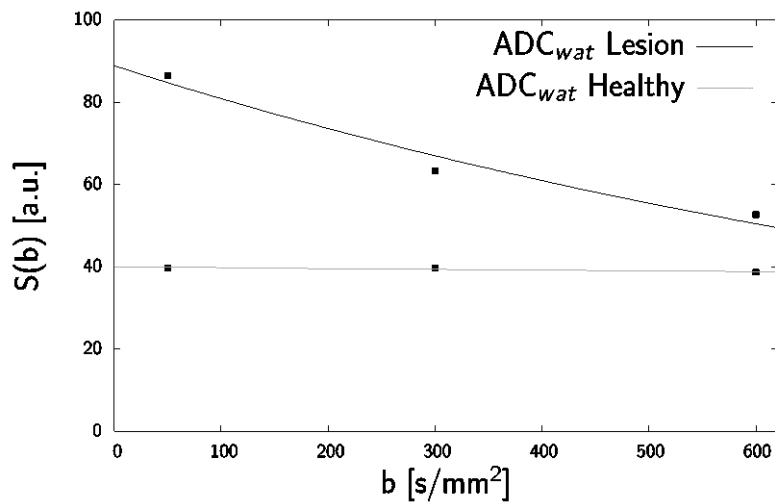
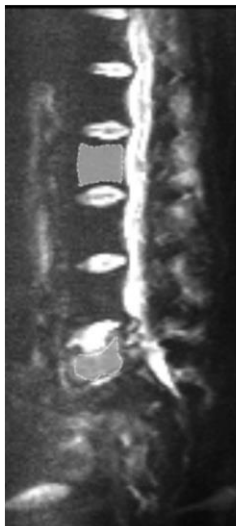


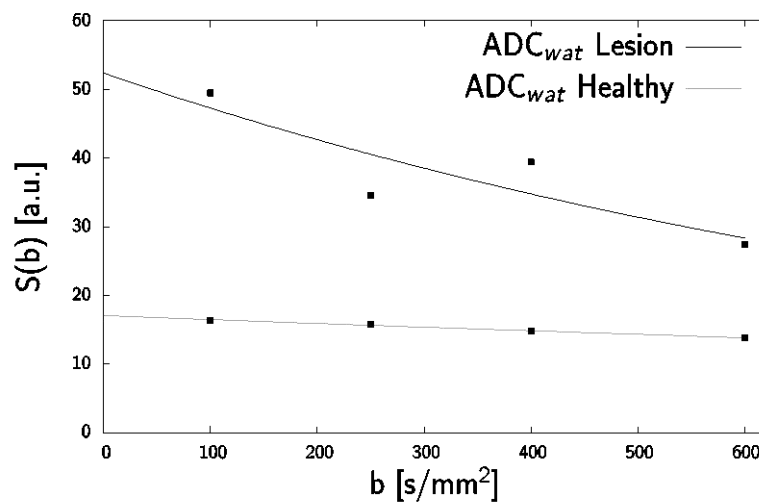
Figure 3: Reference images and the corresponding fits to the signal models for the ROI data. (a) Fit to saturation recovery model, reference image corresponds to the fat-saturated image with TI = 3200 ms; (b) fit to the monoexponential decay model as a function of TE, the reference image corresponds to the fat-saturated image with TE = 14 ms.

Table 2: Summary of p-values of paired and unpaired t-tests for comparisons of ADCs as well as T1 and T2 relaxation times in water. For comparison between normal-appearing vBM and fractures, a paired t-test and in the case of osteoporotic vs. malignant parameters an unpaired t-test was performed. Significant differences ($p < 0.05$) are denoted by bold figures.

t-tests	Parameter	ADC(DW-ssTSE)	ADC(DW-EPI)	T1 water	T2 water
Normal-appearing vBM vs. lesion					
	Osteoporotic (n=20)	<0.0001	<0.0001	<0.0001	<0.0001
	Malignant (n=24)	<0.0001	<0.0001	<0.0001	0.17
Osteoporotic vs. malignant					
	Normal vBM (n=147 vs. 68)	0.63	0.33	0.91	0.15
	Lesion (n=24 vs. 20)	0.0008	0.21	0.20	0.055



(c): DW-EPI



(d): DW-ssTSE

Figure 4: Fits to the monoexponential decay model as a function of the b-value for (a) DW-EPI, the reference image with $b = 50 \text{ s/mm}^2$, and (b) DW-ssTSE, the reference image with $b = 100 \text{ s/mm}^2$.

Table 3: Mean values of the intra-patient variabilities (IPV) of the parameters in normal-appearing bone marrow and of the ratios between the values in the lesion and normal-appearing vBM (Lesion/Normal). The variabilities are given as the percentage of the mean value (standard deviations in parentheses). For the ratios, a significant difference ($p < 0.05$) from the hypothesis Lesion/Normal = 1 is denoted by bold figures.

Parameter	ADC(DW-ssTSE)	ADC(DW-EPI)	T1 water	T2 water	T1 fat	T2 fat
IPV [%]						
malignant osteoporotic	15.2 (8.4)	35.1 (23.2)	10.5 (9.3)	11.3 (8.6)	24.8 (20.3)	11.4 (0.6)
	21.0 (13.6)	29.7 (16.0)	11.0 (4.5)	9.6 (5.1)	16.5 (10.2)	9.7 (4.0)
Lesion/Normal						
malignant osteoporotic	2.43 (0.67)	3.57 (1.44)	1.43 (0.19)	1.16 (0.32)	--	--
	3.03 (0.62)	4.25 (1.61)	1.52 (0.23)	1.39 (0.23)	--	--

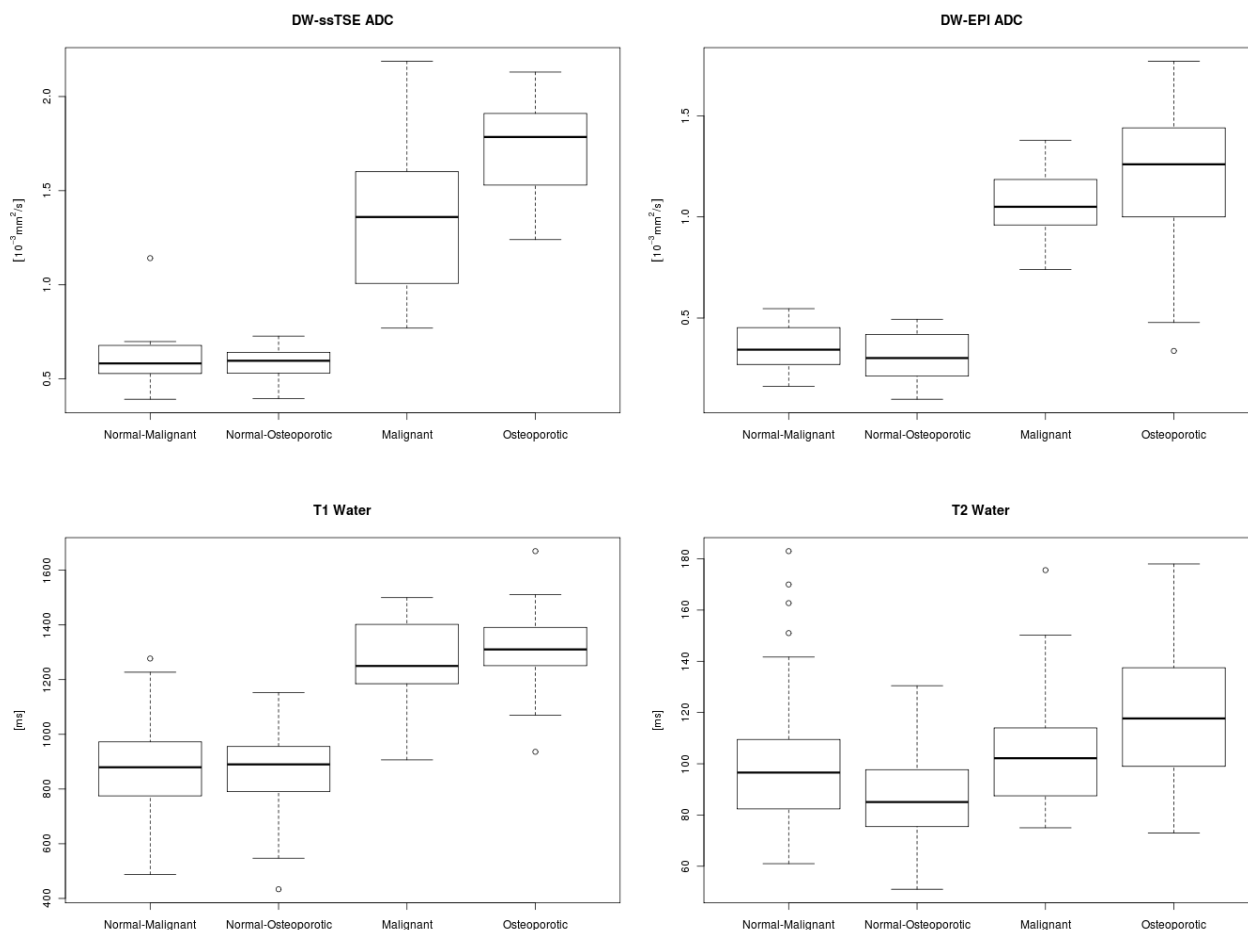


Figure 5: Box plots summarising the values of the ADCs determined with the DW-ssTSE (upper left) and the DW-EPI (upper right) and the T1- (lower left) and the T2-values (lower right) of the water component. Shown are the values in normal-appearing vBM and in the lesions of patients with osteoporosis and patients with malignant lesions.

The results for the different parameters are summarised in the box-plots in Fig. 5. The values in normal-appearing vBM and in the lesions of patients with osteoporotic or malignant lesions are shown separately. The mean values and standard deviations corresponding to these plots are summarised in Table 1. In addition, the values of the relaxation times of the fat component in normal-appearing vBM are shown.

Except for the T1 and T2 values of the fat component, which could not be determined in the fractures, the p-values of the comparisons of each parameter between the different subgroups are summarised in Table 2. Significant differences between normal-appearing vBM and the lesions were found in both patient groups for each of the measured parameters ($p < 0.01$), except for T2 of water between normal-appearing vBM in patients with osteoporosis

and malignant lesions ($p = 0.17$). Comparing normal-appearing vBM of both patient groups, no significant differences for any of the parameters were found. In the case of the fractures, only the ADCs determined with the DW-ssTSE differed significantly ($p < 0.001$). The T2 of water exhibited almost significant differences between benign and malignant fractures ($p = 0.055$).

In addition to the analysis of the parameters for the whole patient collective, the intra-patient variabilities of each parameter were calculated and are summarised in Table 3. The smallest IPV (of about 10 %) were found for the T1 and T2 relaxation times in water and for the T2 relaxation times in fat. The highest IPV was found for the ADCs determined with the DW-EPI sequence in normal-appearing vBM of patients with malignant lesions (35.1 %).

Table 4: Summary of Pearson's product-moment correlation coefficients among the different parameters for the different subgroups. Significant correlations ($p < 0.05$) are denoted by bold figures.

Pearson's Product-Moment Correlation Coefficient	Normal-appearing vBM		Lesion	
	Osteoporosis	Malignant	Osteoporosis	Malignant
ADC(DW-ssTSE) vs. ADC(DW-EPI)	0.66	0.43	0.26	0.76
T1 vs. T2	0.18	0.01	0.49	0.52
T1 vs. ADC(DW-ssTSE)	0.51	0.79	0.20	0.31
T2 vs. ADC(DW-ssTSE)	0.25	0.19	-0.11	0.34
T1 vs. ADC(DW-EPI)	0.73	0.35	0.53	0.28
T2 vs. ADC(DW-EPI)	0.30	0.20	0.41	0.36

Table 5: Sensitivities, specificities, accuracies, positive predictive values (PPV), and negative predictive values (NPV) of the different parameters with respect to the diagnosis of a malignant lesion

Parameter	Cut-off	Sensitivity	Specificity	Accuracy
ADC(DW-ssTSE) [10 ⁻³ mm ² /s]	1.49	0.65 (13/20)	0.88 (21/24)	0.77
ADC(DW-EPI) [10 ⁻³ mm ² /s]	1.12	0.68 (13/19)	0.65 (15/23)	0.67
T1-water [ms]	1262	0.6 (12/20)	0.75 (18/24)	0.68
T2-water [ms]	114	0.78 (14/18)	0.67 (16/24)	0.71
ADC(DW-ssTSE) & T2-water	1.29/119*	0.78 (14/18)	0.96 (23/24)	0.88

*cut-off in the combined case corresponds to point on the linear discriminant. All points fulfilling the condition: $-\tan(31^\circ) (T2\text{-water} - 119 \text{ ms}) / (103 \text{ ms}) + (\text{ADC} - 1.29 \times 10^{-3} \text{ mm}^2/\text{s}) / (1.34 \times 10^{-3} \text{ mm}^2/\text{s}) < 0$ are classified as malignant. 103 ms and $1.34 \times 10^{-3} \text{ mm}^2/\text{s}$ correspond to the difference between maximum and minimum of T2 and ADC values in the lesions and were used for normalisation of the data. 31° is the angle between the linear discriminant and the ADC axis.

Furthermore, the parameter ratio between normal-appearing vBM and the lesion were calculated for each patient and parameter. The mean values and standard deviations of these ratios are summarised in **Fehler! Verweisquelle konnte nicht gefunden werden**.³ The ratios differed significantly from 1 ($p < 0.001$) except for the T2 relaxation time in patients with malignant lesions ($p = 0.077$). The highest separation was found for the ADCs measured with the DW-EPI (malignant: 3.57 and osteoporotic: 4.25) and the DW-ssTSE (malignant: 2.43 and osteoporotic: 3.03).

Possible correlations among the different parameters were evaluated and the results of the Pearson's product-moment correlation coefficient among the different parameters in the different subgroups are summarised in Table 4. Significant correlations ($p < 0.05$) were found between the ADCs determined with the DW-ssTSE and DW-EPI sequence in normal-appearing vBM of patients with osteoporosis and in malignant lesions, between T1 and T2 of water in osteoporotic and malignant lesions, T1 of water and DW-ssTSE ADCs in osteoporotic and malig-

nant normal-appearing vBM, and between DW-EPI ADCs in osteoporotic normal-appearing vBM and osteoporotic fractures.

Finally, the specificities and sensitivities of the different parameters for the differentiation between osteoporotic and malignant lesions were analysed; the results are summarised in Table 5. The highest accuracy of 77 % was found for the ADC determined with the DW-ssTSE sequence. For a cut-off value of $1.49 \times 10^{-3} \text{ mm}^2/\text{s}$, a sensitivity of 65% and a specificity of 88% were found. For the other parameters, the accuracies were found to be smaller. Fisher's linear discriminant analysis showed that for a combined classification based on T2 and DW-ssTSE ADC the accuracy could be increased to 88%, corresponding to a sensitivity of 78% and a specificity of 96%. The linear discriminant corresponds to a rotation of the x-axis (corresponding to the ADC) by 31° as shown in Fig. 6. All other combinations of measured parameters did not increase the accuracy compared with the evaluation of the DW-ssTSE ADC alone.

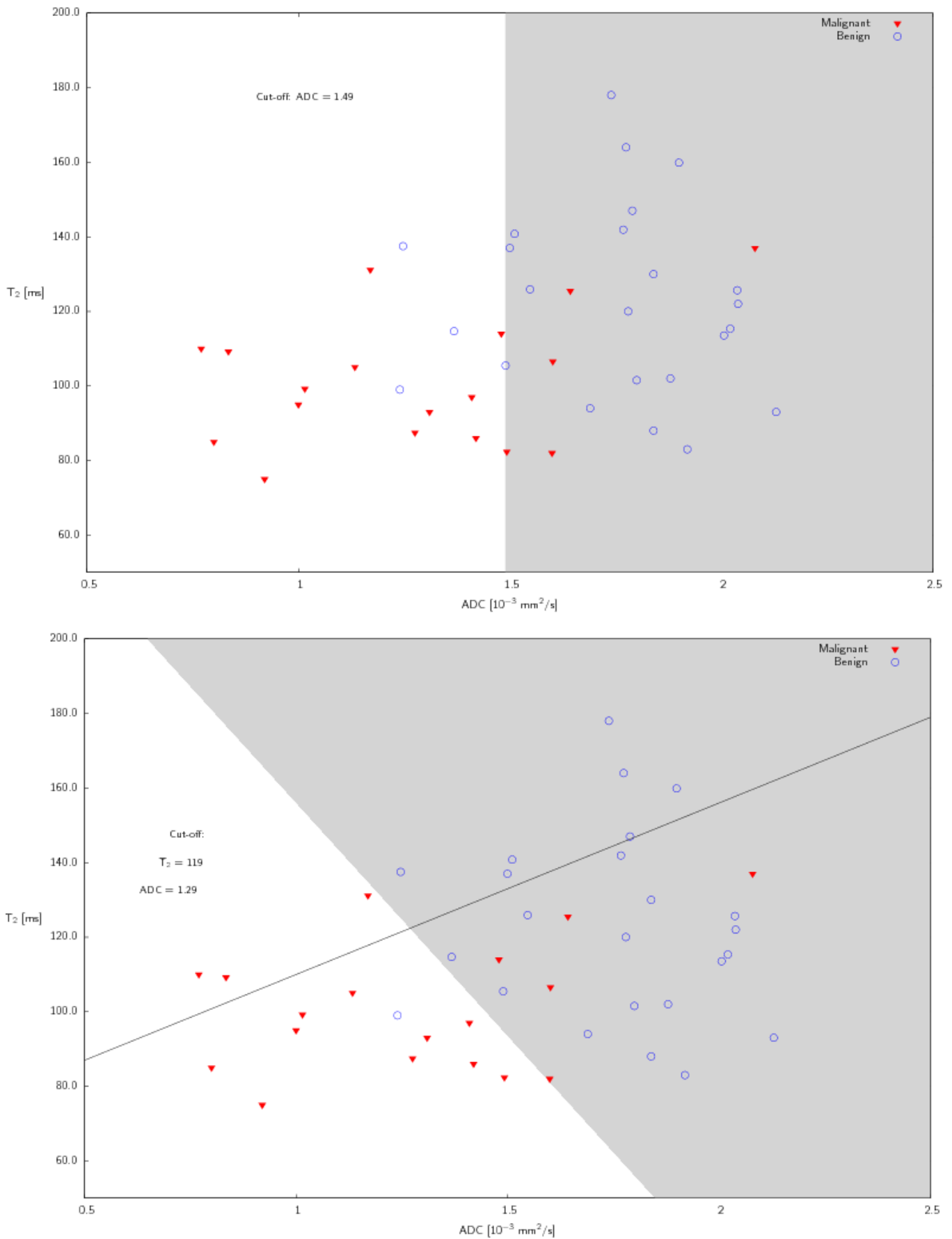


Figure 6: Scatterplots of the ADC(ssTSE) vs. T₂. In the upper figure, the separation between malignant and benign lesions based on the ADC is shown. The white area corresponds to a classification as malignant fractures. In the lower plot, the linear discriminant for a classification based on T₂ and ADC is shown as the black line. The cut-off separating the grey and white areas corresponds to the intersection of the grey border with the linear discriminant.

Discussion

Historically, relaxation times as well as apparent diffusion coefficients of vBM were determined as bulk values, representing a mixture of fat and water. Since the values in fat and water show substantial differences when determining bulk values in different patients and pathological conditions, differences might not only be related to a change in the physical parameter but also to a change in the tissue composition. A separate determination of relaxation times and ADCs for both components might avoid this misinterpretation.

T1 relaxation

T1 of water and fat protons have only been measured in a few studies. Our values for T1 of the water component in normal-appearing vBM of 872 ms in patients with osteoporosis and of 878 ms in patients with malignant infiltration agree with the measurements of Träber et al. at 1.5T [14]. The T1 values of the fat component (386 and 324 ms) are somewhat higher than those of 260–290 ms obtained in [14,15]. The standard deviations and the IPV of T1 in fat are relatively large, possibly caused by partially insufficient water suppression in the present study. Träber et al. performed a spectroscopic measurement, which does not suffer from any imperfect suppression effects. Gold et al. [15] used a spectral-spatial excitation pulse.

It was shown by Sugimura et al. [23] at 0.15T that bulk T1 of malignant metastatic lesions was longer than that of non-neoplastic. Träber et al. at 1.5T reported an increase in T1 of water of 16% in malignant lesions compared with normal vBM [14]. We found an increase of 43% in malignant lesions compared with normal-appearing vBM in the same patient, possibly explained by the higher ratio of free to fixed water in tumours. Ito et al. [36] found a positive correlation between the BMD and T1 of water at 1.5T. Conversely, Träber et al. found no significant differences between normal-appearing vBM of patients with and without osteoporosis. This agrees with our results, showing no significant differences between T1 in normal-appearing vBM of patients with osteoporosis and those with malignant lesions. Here, for the first time, the T1 of water in osteoporotic fractures was determined. It was found to be increased by 52%; possibly, the free water in the bone marrow oedema is responsible for this increase.

T2 relaxation

T2 of water in vBM has previously been measured only by Träber et al.. Our values of 88 ms in normal-appearing vBM of patients with osteoporosis and 99 ms in patients with malignant lesions are about 30 % higher. T2 of fat in vBM was determined by Gold et al. as 166 ms agreeing well with our values in normal-appearing vBM of 163 ms in patients with osteoporosis and 146 ms in patients with malignant lesions. The values reported by Träber et al. of about 70 ms are 50% smaller than our results. Interestingly, the T2 values of fat measured by Gold et al. agree, while the T1 values of fat disagree with our results although the same technique of fat suppression was applied in both cases [15].

In malignant lesions, an increase of 16% of T2 was found compared with normal-appearing vBM. These differences were not significant, contrary to the findings of Träber et al. reporting a significant difference ($p < 0.002$). T2 in osteoporotic fractures have not been determined before. A significant increase of 39% was found, possibly caused by a reduction of local magnetic field gradients caused by the destruction of the trabecular structure.

Apparent diffusion coefficients

Typical ADCs in the literature vary from 0.2 to $0.5 \times 10^{-3} \text{ mm}^2/\text{s}$ [37]. The general variability can be explained by the different pulse sequences and diffusion weightings used. The most important difference is the application of fat saturation; typical values with fat saturation are in the range of 0.3 to $0.5 \times 10^{-3} \text{ mm}^2/\text{s}$. Our ADCs obtained with the DW-ssTSE and DW-EPI differ significantly. The SNR of the DW-ssTSE sequence at higher b-values was higher than that of the DW-EPI sequence. Thus, the signal attenuation of the DW-EPI sequence is underestimated yielding lower estimates for the ADCs. Furthermore, the DW-EPI images suffered from gross geometrical image distortions, caused by susceptibility heterogeneities. Because of these limitations, the DW-ssTSE appears to be the preferable sequence in the vertebral column.

In the lesions, the ADCs are substantially increased compared with normal-appearing vBM. The effect of the underestimation of ADCs is more important in normal-appearing vBM, thus the ratios between lesion and normal-appearing vBM are higher for the DW-EPI sequence.

Lesion differentiation

We investigated the potential of the various parameters determined in this study for the differentiation. The only parameter that provided a significant difference was the ADC, which is in agreement with previous studies [25-27, 30, 31, 38, 39]. However, an overlap between the two groups exists and, therefore, the sensitivity (65 %) and the specificity (88 %) are not high enough to replace the usual diagnosis based on the histological validation. An improvement of the diagnostic accuracy compared with each of the evaluated parameters alone was possible when ADC and T2 were combined. Using the linear discriminant based on T2 and ADC, we obtained a sensitivity of 78% and a specificity of 96%. This value is lower than the values reported based on the differentiation based on qualitative criteria [16-22], which might partially be explained by the relatively low number of patients included in the present study. However, quantitative parameters might provide additional information especially in the cases where the cause of the fracture is not apparent on conventional MR imaging. The combination of qualitative and quantitative criteria might provide the best differentiation in these cases.

Non-quantitative diffusion-weighted imaging has also been successfully applied for lesion differentiation using diffusion-weighted steady-state free-precession (DW-SSFP) sequences [40-45]. The signal of the DW-SSFP sequence is a very complex function of the ADCs and the relaxation times [46]. The exact contrast mechanism resulting in the excellent lesion differentiation is not yet fully understood. The parameters quantified in the present study might be important input parameters for a better understanding of the different signal behaviour of the DW-SSFP sequence.

Conclusion

For the first time, vertebral T1 and T2 relaxation times of the fat and water components and ADCs were measured in patients presenting with vertebral lesions. All parameters exhibit significant differences between normal-appearing vBM and the lesions. However, only the ADCs determined with a DW-ssTSE technique showed significant differences between osteoporotic fractures and malignant lesions and might be helpful for the differential diagnosis of these two entities.

Acknowledgements

This work was supported by the Deutsche Forschungsgemeinschaft (DFG), grant no. DI 1413/1-1.

References

1. Vogler JB, Murphy WA (1988) Bone marrow imaging. *Radiology* 168:679-693
2. Wehrli F W, MacFall J R, Shutts D et al (1984) Mechanisms of contrast in NMR imaging. *J Comput Assist Tomogr* 8:369-380.
3. Vande Berg C V, Malghem J, Lecouvet F E et al (1998) Magnetic resonance imaging of the normal bone marrow. *Skeletal Radiol* 27:471-483.
4. Bottomley P A, Foster T H, Argersinger R E et al (1984) A review of normal tissue hydrogen NMR relaxation times and relaxation mechanisms from 1-100 MHz: dependence on tissue type, NMR frequency, temperature, species, excision, and age. *Med Phys* 11:425-448.
5. Doms G C, Fisher M R, Hricak H et al (1985) Bone marrow imaging: magnetic resonance studies related to age and sex. *Radiology* 155:429-432.
6. Richards M A, Webb J A, Jewell S E (1988) In-vivo measurement of spin lattice relaxation time (T1) of bone marrow in healthy volunteers: the effects of age and sex. *Br J Radiol* 61:30-33.
7. De Bazelaire C M J, Duhamel G, Rofsky N M et al (2004) MR imaging relaxation times of abdominal and pelvic tissues measured in vivo at 3.0 T: preliminary results. *Radiology* 230: 652-659.
8. Dietrich O, Herlihy A, Dannels W R et al (2001) Diffusion-weighted imaging of the spine using radial k-space trajectories. *MAGMA* 12:23-31.
9. Byun W M, Shin S O, Chang Y et al (2002) Diffusion-weighted MR imaging of metastatic disease of the spine: assessment of response to therapy. *AJNR Am J Neuroradiol* 23:906-912.
10. Bammer R, Herneth A M, Maier S E et al (2003) Line scan diffusion imaging of the spine. *AJNR Am J Neuroradiol* 24:5-12.
11. Yeung D K W, Wong S Y S, Griffith J F et al (2004) Bone marrow diffusion in osteoporosis: evaluation with quantitative MR diffusion imaging. *J Magn Reson Imaging* 19:222-228.
12. Griffith J F, Yeung D K W, Antonio G E et al (2006) Vertebral marrow fat content and diffusion and perfusion indexes in women with varying bone density: MR evaluation. *Radiology* 241:831-838.
13. Ward R, Caruthers S, Yablon C et al (2000) Analysis of diffusion changes in posttraumatic bone marrow using navigator-corrected diffusion gradients. *AJR Am J Roentgenol* 174:731-734.
14. Träber F, Block W, Layer G et al (1996) Determination of 1H relaxation times of water in human bone marrow by fat-suppressed turbo spin echo in comparison to MR spectroscopic methods. *J Magn Reson Imaging* 6:541-548.
15. Gold G E, Han E, Stainsby J et al (2004) Musculoskeletal MRI at 3.0 T: relaxation times and image contrast. *AJR Am J Roentgenol* 183:343-351.
16. Frager D, Elkin C, Swerdlow M (1988) Subacute osteoporotic compression fracture: misleading magnetic resonance appearance. *Skeletal Radiol* 17:123-126.
17. Yuh W T, Zachar C K, Barloon T J et al (1989) Vertebral compression fractures: distinction between benign and malignant causes with MR imaging. *Radiology* 172:215-218.
18. Baker L L, Goodman S B, Perkash I (1990) Benign versus pathologic compression fractures of vertebral bodies:

- assessment with conventional spin-echo, chemical-shift, and STIR MR imaging. *Radiology* 174:495-502.
19. Rupp R E, Ebraheim N A and Coombs R J (1995) Magnetic resonance imaging differentiation of compression spine fractures or vertebral lesions caused by osteoporosis or tumor. *Spine* 20:499-503.
 20. Cuenod C A, Laredo J D, Chevret S, et al (1996) Acute vertebral collapse due to osteoporosis or malignancy: appearance on unenhanced and gadolinium-enhanced MR images. *Radiology* 199:541-549.
 21. Shih T T, Huang K M and Li Y W (1999) Solitary vertebral collapse: distinction between benign and malignant causes using MR patterns. *J Magn Reson Imaging* 9:635-642.
 22. Jung H, Jee W, McCauley T R, et al (2003) Discrimination of metastatic from acute osteoporotic compression spinal fractures with MR imaging. *Radiographics* 23:179-187.
 23. Sugimura K, Yamasaki K, Kitagaki H et al (1987) Bone marrow diseases of the spine: differentiation with T1 and T2 relaxation times in MR imaging. *Radiology* 165:541-544.
 24. Sundaram M, McGuire M H and Schajowicz F (1987) Soft-tissue masses: histologic basis for decreased signal (short T2) on T2-weighted MR images. *AJR Am J Roentgenol* 148:1247-1250.
 25. Herneth A M, Naude J, Philipp M et al (2000) The value of diffusion-weighted MRT in assessing the bone marrow changes in vertebral metastases. *Radiologe* 40:731-736.
 26. Chan J H M, Peh W C G, Tsui E Y K et al (2002) Acute vertebral body compression fractures: discrimination between benign and malignant causes using apparent diffusion coefficients. *Br J Radiol* 75:207-214.
 27. Zhou X J, Leeds N E, McKinnon G C et al (2002) Characterization of benign and metastatic vertebral compression fractures with quantitative diffusion MR imaging. *AJNR Am J Neuroradiol* 23:165-170.
 28. Maeda M, Sakuma H, Maier S E et al (2003) Quantitative assessment of diffusion abnormalities in benign and malignant vertebral compression fractures by line scan diffusion-weighted imaging. *AJR Am J Roentgenol* 181:1203-1209.
 29. Oner A Y, Tali T, Celikyay F et al (2007) Diffusion-weighted imaging of the spine with a non-Carr-Purcell-Meiboom-Gill single-shot fast spin-echo sequence: initial experience. *AJNR Am J Neuroradiol* 28: 575-580.
 30. Raya J G, Dietrich O, Birkenmaier C et al (2007) Feasibility of a RARE-based sequence for quantitative diffusion-weighted MRI of the spine. *Eur Radiol* 17:2872-2879.
 31. Balliu E, Vilanova J C, Peláez I et al (2009) Diagnostic value of apparent diffusion coefficients to differentiate benign from malignant vertebral bone marrow lesions. *Eur J Radiol* 69:560-566.
 32. Sourbron S, Biffar A, Ingrischi M et al (2009) PMI: Platform for Research in Medical Imaging. ESMRMB09 Antalya, 2009.
 33. Crawley A P and Henkelman R M (1988) A comparison of one-shot and recovery methods in T1 imaging. *Magn Reson Med* 7:23-34.
 34. Abragam A (2004) Principles of nuclear magnetism. New York, Oxford University Press.
 35. Stejskal E O and Tanner J E (1965) Spin Diffusion Measurements: Spin Echoes in the Presence of a Time-Dependent Field Gradient. *J Chem Phys* 42:288-292.
 36. Ito M, Hayashi K, Uetani M et al (1993) Bone mineral and other bone components in vertebrae evaluated by QCT and MRI. *Skeletal Radiol* 22:109-113.
 37. Dietrich O, Biffar A, Reiser M et al (2009) Diffusion-weighted imaging of bone marrow. *Semin Musculoskelet Radiol* 13:134-144.
 38. Herneth A, Philipp M, Naude J et al (2002) Vertebral metastases: assessment with apparent diffusion coefficient. *Radiology* 225:889-894.
 39. Tang G, Liu Y, Li W et al (2007) Optimization of b value in diffusion-weighted MRI for the differential diagnosis of benign and malignant vertebral fractures. *Skeletal Radiol* 36:1035-1041.
 40. Baur A, Stähler A, Brüning R et al (1998) Diffusion-weighted MR imaging of bone marrow: differentiation of benign versus pathologic compression fractures. *Radiology* 207:349-356.
 41. Abanoz R, Hakyemez B and Parlak M (2003) Diffusion-weighted imaging of acute vertebral compression: Differential diagnosis of benign versus malignant pathologic fractures. *Tani Girisim Radyol* 9:176-183.
 42. Hackländer T, Scharwächter C, Golz R et al (2006). Value of diffusion-weighted imaging for diagnosing vertebral metastases due to prostate cancer in comparison to other primary tumors. *Rofo* 178:416-424.
 43. Byun W M, Jang H W, Kim S W et al (2007) Diffusion-weighted magnetic resonance imaging of sacral insufficiency fractures: comparison with metastases of the sacrum. *Spine* 32:820-824.
 44. Castillo M, Arbelaez A, Smith J K et al (2000) Diffusion-weighted MR imaging offers no advantage over routine noncontrast MR imaging in the detection of vertebral metastases. *AJNR Am J Neuroradiol* 21:948-953.
 45. Baur A, Huber A, Dürr HR et al (2002) Differentiation of benign osteoporotic and neoplastic vertebral compression fractures with a diffusion-weighted, steady-state free precession sequence. *Rofo* 174:70-75.
 46. Buxton R B (1993) The diffusion sensitivity of fast steady-state free precession imaging. *Magn Reson Med* 29:235-243.